

# Solar Cycle Variation of Axial Orientations and Favorable Locations of Eruptive MFRs

Hong Xie<sup>1,2</sup>, Nat Gopalswamy<sup>1</sup>, Sachiko Akiyama<sup>1,2</sup>, Pertti Makela<sup>1,2</sup>, and Seiji Yashiro<sup>1,2</sup>

<sup>1</sup>NASA Goddard Space Flight Center, 8800 Greenbelt Road Greenbelt, MD, 20771, USA  
email: [hong.xie@nasa.gov](mailto:hong.xie@nasa.gov)

<sup>2</sup>The Catholic University of America, 620 Michigan Avenue, N.E. Washington, DC 20064, USA

**Abstract.** Using multi-viewpoint observations from STEREO and SOHO during three solar cycles from 23 to 25, we study the magnetic flux rope (MFR) structures of coronal mass ejections (CMEs) near the Sun and magnetic clouds (MCs) at 1au. The study aims to investigate two phenomena: 1) the occurrence rate of CMEs near Hale sector boundaries (HBs) and 2) solar-cycle variation of MFR axial orientations in CMEs and MCs. Our preliminary results include: 1) the axes of MFRs in cycle 25 present a systematic northward orientation, which is the same as in cycle 23 but opposite to cycle 24; 2) the majority of the MFRs occurred near HBs (within 30 degrees) and some exceptional events occurred at non-HBs; 3) the axial fields in MCs present a similar north-south orientation, which changes from cycle to cycle. We discuss the implication of solar cycle variations of MFR axial orientations for space weather forecasts.

**Keywords.** Hale polarity law, Hale boundary, magnetic flux ropes, coronal mass ejections

---

## 1. Introduction

Since the start of the previous century, solar observations have revealed that active regions (ARs) spot polarities present a systematic east-west orientation that reverses in opposite hemispheres and across odd and even cycles (Hale's law, [Hale & Nicholson 1925](#)). They also present a north-south orientation, i.e., the leading spots appear closer to the equator than the following spots do and the tilt of the spots with opposite polarities grows with the latitude of AR to facilitate the polar field reversal in each cycle (Joy's law, [Hale et al. 1919](#)).

Solar eruptions, such as flares and coronal mass ejections (CMEs), are also influenced by large-scale neutral lines in the solar corona, i.e., the boundaries between opposite magnetic poles ([Wilcox & Ness 1965](#)). [Svalgaard et al. \(1975\)](#) showed that the sector boundary observed in magnetic fields at Earth can be mapped back to the large-scale neutral line in the photosphere and in the solar corona. [Svalgaard & Wilcox \(1976\)](#); [Svalgaard et al. \(2011\)](#) found that magnetic field fluxes tend to emerge near the Hale sector boundary (HB hereafter), and suggested a link between the HB effect to the deep interior of the Sun. A number of other studies have also found that flares and most complex CME-productive ARs tend to occur near the HB (e.g. [Getachew et al. 2017](#); [Gyenge et al. 2017](#); [Loumou et al. 2018](#)).

The magnetic flux rope (MFR) axial field in bipolar ARs and filament channels (FLs) can be approximated by the tilt of polarity inversion lines (PILs) between opposite polarities. Recent studies have shown that most CMEs and magnetic clouds (MCs) contain the MFR structures (e.g. [Gopalswamy et al. 2013](#); [Xie et al. 2013](#); [Vourlidis 2014](#)); and the axial tilts of CMEs and MCs are well correlated with the PILs of their source regions (e.g. [Marubashi et al. 2015](#); [Xie et al. 2021](#)). Similar cycle variations have been found in MC axial tilts at 1au (e.g. [Bothmer & Rust 1997](#); [Gopalswamy et al. 2015](#); [Lepping et al. 2011](#)). In this paper, we investigate the solar-cycle variation of the MFR axial orientation and the relationship between HBs, PIL tilts and CME eruptions. The study aims to answer two questions: 1) how frequently or at what rate

do CMEs erupt at HBs? 2) How does the solar-cycle variation of axial orientation of MFRs affect geomagnetic activity?

## 2. Data and Event Selection

Seventy-seven MC-CMEs during the first four years of three cycles from 23 to 25 have been used in this study. Events in cycles 23 and 24 are selected from Xie et al. (2021), where we have excluded complex events involving successive CMEs. The selected MC-CME pairs are divided into three types, i.e., stealth CMEs, CMEs associated with flares (flare CMEs), and CMEs associated with filaments (filament CMEs). In Table 1, we list the number of CMEs in each cycle and CME types.

**Table 1.** Numbers of MC-CMEs associated with three source types

	Total	Stealth CMEs	Flare CMEs	Filament CMEs
SC 23	26	7	11	8
SC 24	27	7	9	11
SC 25	24	7	8	9

To identify the MFR sources and PIL tilts, we used extreme ultraviolet (EUV) images from the Atmospheric Imaging Assembly (AIA; Lemen et al. 2012) and magnetograms from the Helioseismic and Magnetic Imager (HMI; Scherrer et al. 2012) aboard the Solar Dynamics observatory (SDO; Pesnell et al. 2012). For stealth CMEs, since the associated EUV and magnetogram signatures are too faint, we apply a flux-rope fit to determine their source locations, we then use the coronal neutral line (CNL) tilt combined with the hemispheric helicity rule as a proxy for the PIL orientation (see details in Xie et al. 2021).

## 3. Results and Discussion

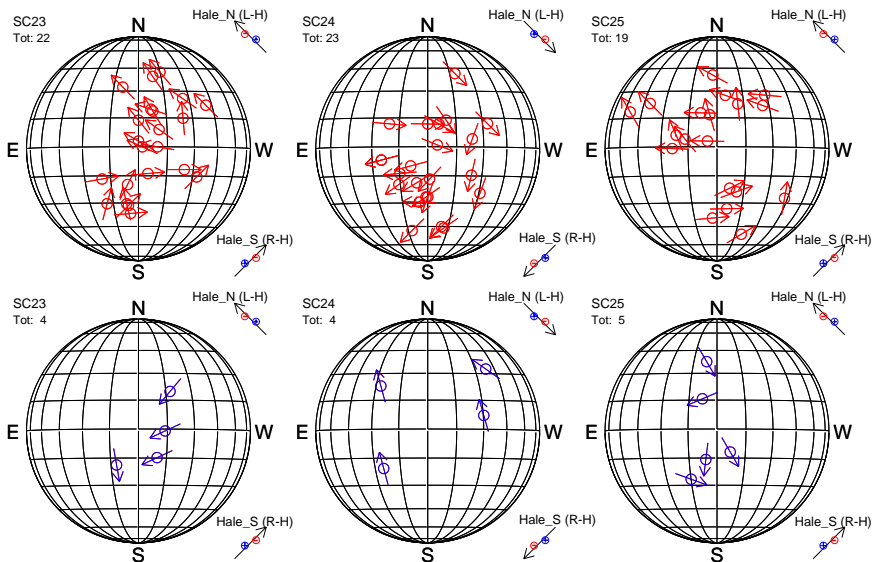


**Figure 1.** Comparison of PIL tilts for Hale and non-Hale source regions during odd cycles (23 and 25) and even cycle 24.

Figure 1 shows distributions of the MFR tilts for each cycle: (top) Hale CMEs and (bottom) non-Hale CMEs, where Hale (non-Hale) CMEs refer to cases when associated source polarities are following (against) the Hale’s polarity law. We can see that, for all three cycles, the

majority of the CMEs ( $\sim 83\%$ ) are Hale-CMEs. It is shown that during odd (even) cycles, the Hale MFR axial field has a systematic northward (southward) component. In cycles 23 and 25, the Hale MFR axial directions in the northern hemisphere are northeast with a negative helicity (left-handed), and northwest in the southern hemisphere with a positive helicity (right-handed). In even cycle 24, the Hale MFR axial tilts are opposite to the odd cycle, i.e., change to southwest and southeast directions.

In Figure 2, we study the relative position of CME sources to the HB, where we overplot the CME source location (red circle) on the Wilcox Solar Observatory (WSO) source surface map, and HBs are marked by thick purple lines. Here HB refers to the portion of a sector boundary where the polarity change across its neutral line matches that in bipolar source regions (ARs of FLs).

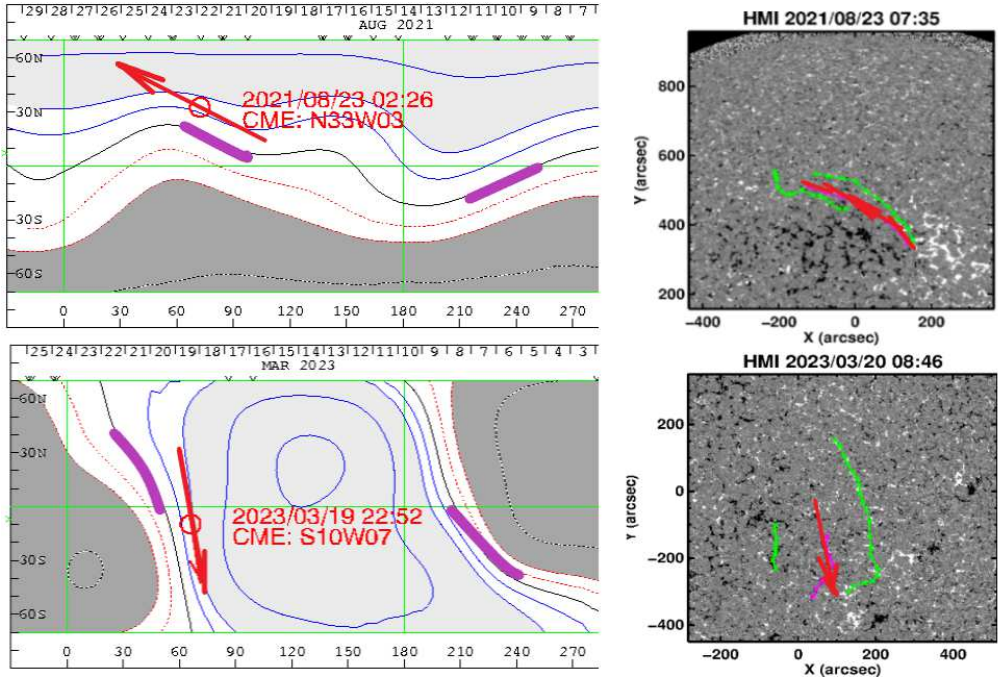


**Figure 2.** (Left) WSO source surface synoptic maps calculated for a height of 2.5 Rs. Dark gray contours represent negative (-) fields, light gray contours, positive (+) fields. The black solid line is the CNL. The CME source locations (red circles), PILs (red arrows) and HBs (thick purple lines) are overplotted on the maps. (Right) The CME PILs and post-eruption arcade footpoints (green lines) overplotted on the HMI magnetograms.

Figure 2 shows (top) an example of a Hale MFR on 2021 Aug 23 and (bottom) a non-Hale MFR on 2023 Mar 19. In Figure 2 top panels, the associated CME erupted near a northern HB, resulting in a northeast left-handed MC at 1 au, while in Figure 2 bottom panels, a CME occurred near a southern non-HB, leading to a southward right-handed MC and well-known geomagnetic storm on 2023 Mar 24 during cycle 25 (e.g. Rajana et al. 2024; Paul et al. 2024).

By comparing the CME and HB locations, we found that  $\sim 74\%$  of the MC-CMEs in our dataset erupted near HBs (within  $\pm 30^\circ$ );  $\sim 26\%$  of CME-MCs occurred at the non-HBs, suggesting that HB is one of the locations favorable to CME eruption. The non-HB CMEs tend to occur at inter-Hale ARs (FLs) source regions and/or complex ARs accompanied with new emerging fluxes.

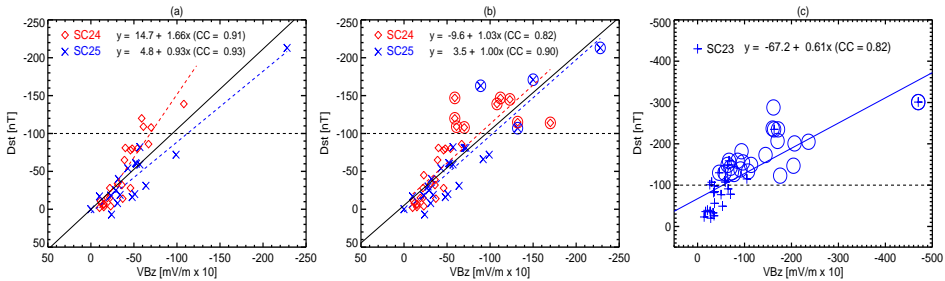


**Figure 3.** (a) Correlation between  $VB_z$  and Dst during cycles 24 (red diamond) and 25 (blue 'x'), (b) same as (a), with major geomagnetic storms added, marked by red and blue circles for the two cycles, and (c) correlation between  $VB_z$  and Dst (blue cross) with major geomagnetic storms (blue circles) during cycle 23.

To discuss the effect of solar cycle variation of MFR axial orientations on geomagnetic activity, in Figure 3a, we compare the correlations between solar wind electric field ( $VB_z$ ) and Dst index for Hale MC-CMEs during cycle 24 (red diamond) and 25 (blue 'x'). It shows that the fitted slope in cycle 24 is  $\sim 1.8$  times larger than in cycle 25, i.e., 1.66 vs 0.93, suggesting that an even cycle with a prevailing southward axial field is more geoeffective than an odd cycle. There are 9 major geomagnetic storms during the first four years of cycle 24 and only 4 major storms in cycle 25 from 2020 to 2023. In Figure 3b, we overplotted all the major geomagnetic storms with  $Dst < -100$  nT (marked by red and blue circles) for the two cycles. Table 2 lists the number of major geomagnetic storms, where the storms are grouped as ejecta, sheath, Hale-MC and non-Hale MC storms, respectively. It is shown that the difference of fit-slopes for the two cycles has been smoothed out after adding ejecta, sheath and non-Hale storms. During cycle 24, 4 out of 9 major storms are caused by the southward Hale MCs, 3 are associated with ejectas and 2 are sheath storms. During cycle 25, 2 storms are caused by shock sheaths, 1 by a low-inclination MC (with a tilt  $\sim 20^\circ$ ), 1 by a southward non-Hale MC.

Note that, the geoeffective activity is not only affected by the MC axial orientation but also the solar cycle strength, i.e., the solar wind electric field. As shown in Figure 3c, during an "active" cycle, the stronger cycle 23 has more number of major geomagnetic storms than both weaker cycles 24 and 25 due to the large  $VB_z$ . The geoeffectiveness during an active cycle may be enhanced due to interactions with other interplanetary magnetic structures, primarily due to the compression of the existing  $B_z$  magnetic field component (e.g. [Farrugia et al. 2006](#); [Lugaz et al. 2017](#)).

**Table 2.** Numbers of different major geomagnetic storms during two cycles

	Total	MC storms		Ejecta storms	Sheath storms
		Hale	non-Hale		
SC 24	9	4	0	3	2
SC 25	4	2	1	0	2

## 4. Conclusions

1) The MFR PILs of cycle 25 present a systematic northward orientation as in cycle 23 but opposite to cycle 24 (southward orientation). This cycle variation may explain that, although cycle 25 is slightly stronger, it contains a relatively weaker geomagnetic activity than cycle 24 during its first four years. 2)  $\sim 74\%$  CME-MCs erupted near HBs (within  $30^\circ$ ), suggesting HB is one of the locations favorable to CME eruption.

We thank SOHO, STEREO, and SDO teams for making their data available online. H.X., S.A., and S.Y. are partially supported by NSF grant AGS-2228967. P.M. is partially supported by NSF grant AGS-2043131.

## References

- Bothmer, V., & Rust, D. 1997, The Field Configuration of Magnetic Clouds and the Solar Cycle (American Geophysical Union (AGU)), 139–146, doi: <https://doi.org/10.1029/GM099p0139>
- Farrugia, C. J., Jordanova, V. K., Thomsen, M. F., et al. 2006, *Journal of Geophysical Research (Space Physics)*, 111, A11104, doi: [10.1029/2006JA011893](https://doi.org/10.1029/2006JA011893)
- Getachew, T., Virtanen, I., & Mursula, K. 2017, *Solar Phys.*, 292, 174, doi: [10.1007/s11207-017-1198-9](https://doi.org/10.1007/s11207-017-1198-9)
- Gopalswamy, N., Nieves-Chinchilla, T., Hidalgo, M., et al. 2013, *Solar Phys.*, 284, 1, doi: [10.1007/s11207-013-0280-1](https://doi.org/10.1007/s11207-013-0280-1)
- Gopalswamy, N., Yashiro, S., Xie, H., Akiyama, S., & Mäkelä, P. 2015, *Journal of Geophysical Research (Space Physics)*, 120, 9221, doi: [10.1002/2015JA021446](https://doi.org/10.1002/2015JA021446)
- Gyenge, N., Singh, T., Kiss, T. S., Srivastava, A. K., & Erdélyi, R. 2017, *ApJ*, 838, 18, doi: [10.3847/1538-4357/aa62a8](https://doi.org/10.3847/1538-4357/aa62a8)
- Hale, G. E., Ellerman, F., Nicholson, S. B., & Joy, A. H. 1919, *ApJ*, 49, 153, doi: [10.1086/142452](https://doi.org/10.1086/142452)
- Hale, G. E., & Nicholson, S. B. 1925, *ApJ*, 62, 270, doi: [10.1086/142933](https://doi.org/10.1086/142933)
- Lemen, J. R., Title, A. M., Akin, D. J., et al. 2012, *Solar Phys.*, 275, 17, doi: [10.1007/s11207-011-9776-8](https://doi.org/10.1007/s11207-011-9776-8)
- Lepping, R. P., Wu, C. C., Berdichevsky, D. B., & Szabo, A. 2011, *Solar Phys.*, 274, 345, doi: [10.1007/s11207-010-9646-9](https://doi.org/10.1007/s11207-010-9646-9)
- Loumou, K., Hannah, I. G., & Hudson, H. S. 2018, *A&A*, 618, A9, doi: [10.1051/0004-6361/201731050](https://doi.org/10.1051/0004-6361/201731050)
- Lugaz, N., Temmer, M., Wang, Y., & Farrugia, C. J. 2017, *Solar Phys.*, 292, 64, doi: [10.1007/s11207-017-1091-6](https://doi.org/10.1007/s11207-017-1091-6)
- Marubashi, K., Akiyama, S., Yashiro, S., et al. 2015, *Solar Phys.*, 290, 1371, doi: [10.1007/s11207-015-0681-4](https://doi.org/10.1007/s11207-015-0681-4)
- Paul, K. S., Haralambous, H., & Oikonomou, C. 2024, *Advances in Space Research*, 73, 6029, doi: [10.1016/j.asr.2024.03.026](https://doi.org/10.1016/j.asr.2024.03.026)
- Pesnell, W. D., Thompson, B. J., & Chamberlin, P. C. 2012, *Solar Phys.*, 275, 3, doi: [10.1007/s11207-011-9841-3](https://doi.org/10.1007/s11207-011-9841-3)
- Rajana, S. S. K., Panda, S. K., Jade, S., et al. 2024, *Ap&SS*, 369, 3, doi: [10.1007/s10509-024-04268-9](https://doi.org/10.1007/s10509-024-04268-9)
- Scherrer, P. H., Schou, J., Bush, R. I., et al. 2012, *Solar Phys.*, 275, 207, doi: [10.1007/s11207-011-9834-2](https://doi.org/10.1007/s11207-011-9834-2)
- Svalgaard, L., Hannah, I. G., & Hudson, H. S. 2011, *ApJ*, 733, 49, doi: [10.1088/0004-637X/733/1/49](https://doi.org/10.1088/0004-637X/733/1/49)
- Svalgaard, L., & Wilcox, J. M. 1976, *Solar Phys.*, 49, 177, doi: [10.1007/BF00221492](https://doi.org/10.1007/BF00221492)
- Svalgaard, L., Wilcox, J. M., Scherrer, P. H., & Howard, R. 1975, *Solar Phys.*, 45, 83, doi: [10.1007/BF00152219](https://doi.org/10.1007/BF00152219)
- Vourlidas, A. 2014, *Plasma Physics and Controlled Fusion*, 56, 064001, doi: [10.1088/0741-3335/56/6/064001](https://doi.org/10.1088/0741-3335/56/6/064001)
- Wilcox, J. M., & Ness, N. F. 1965, *JGR*, 70, 5793, doi: [10.1029/JZ070i023p05793](https://doi.org/10.1029/JZ070i023p05793)
- Xie, H., Gopalswamy, N., & Akiyama, S. 2021, *ApJ*, 922, 64, doi: [10.3847/1538-4357/ac23cc](https://doi.org/10.3847/1538-4357/ac23cc)
- Xie, H., Gopalswamy, N., & St. Cyr, O. C. 2013, *Solar Phys.*, 284, 47, doi: [10.1007/s11207-012-0209-0](https://doi.org/10.1007/s11207-012-0209-0)